mathematics

Article

A New Active Contour Medical Image Segmentation Method Based on Fractional Varying-Order Differential

Yanshan Zhang [1] and Yuru Tian [2,*]

[1] School of Intelligent Engineering, Zhengzhou University of Aeronautics, 15 Wenyuan West Road, Zhengdong New District, Zhengzhou 450015, China; yanshan@zua.edu.cn
[2] Qingdao Institute of Software, College of Computer Science and Technology, China University of Petroleum, 66 Changjiang West Road, Huangdao District, Qingdao 266580, China
* Correspondence: s20070037@s.upc.edu.cn

Abstract: Image segmentation technology is dedicated to the segmentation of intensity inhomogeneous at present. In this paper, we propose a new method that incorporates fractional varying-order differential and local fitting energy to construct a new variational level set active contour model. The energy functions in this paper mainly include three parts: the local term, the regular term and the penalty term. The local term combined with fractional varying-order differential can obtain more details of the image. The regular term is used to regularize the image contour length. The penalty term is used to keep the evolution curve smooth. True positive (TP) rate, false positive (FP) rate, precision (P) rate, Jaccard similarity coefficient (JSC), and Dice similarity coefficient (DSC) are employed as the comparative measures for the segmentation results. Experimental results for both synthetic and real images show that our method has more accurate segmentation results than other models, and it is robust to intensity inhomogeneous or noises.

Keywords: fractional calculus; varying-order differential; active contour; image segmentation; intensity inhomogeneous image

Citation: Zhang, Y.; Tian, Y. A New Active Contour Medical Image Segmentation Method Based on Fractional Varying-Order Differential. *Mathematics* **2022**, *10*, 206. https://doi.org/10.3390/math10020206

Academic Editor: Martin Bohner

Received: 6 December 2021
Accepted: 5 January 2022
Published: 10 January 2022

1. Introduction

The fractional-order PDE (partial differential equation) is an important branch of mathematical analysis, but it is little known by engineering scholars. The fractional order differential has the characteristics of increasing the high frequency component of the signal while preserving the low frequency component of the signal nonlinearly. Most images have rich local features such as texture and detail, and the gray values between pixels in the neighborhood have great similarity. Traditional integer-order differential operations have overall properties to matrix functions such as images. Directly performing an integer-order differential correlation algorithm on images can cause images to appear as blocks or ladders, so it cannot get satisfactory results. Therefore, we think that the fractional order differential can be used to enhance the detailed features of complex texture in two-dimensional image signals. Recently, some scholars have started the application of fractional order differential in image segmentation. Li et al. proposed a novel active contour model based on an adaptive fractional order differential to solve the impact of noise on the image in the process of segmentation [1]. Ren presented a new adaptive active contour model based on fractional order differential [2]. Chen et al. proposed an adaptive-weighting active contour model, which incorporates image gradient, local environment and global information into a framework [3]. Mathieu et al. used a fractional derivative to detect the image edges [4]. On the basis of fractional order differential and our application to other image processing algorithms [5–7], we proposed a fractional varying-order differential, which can simultaneously perform different fractional orders differential operations on each element function of a matrix function, i.e., the differential orders of different parts of the image can be variable. Thus, we can gain more detailed image information so that we can process it conveniently.

Active contour methods can be divided into edge-based model and region-based model. The curve evolution of edge-based active contour models generally uses image gradient information. It can locate the edge accurately by detecting the gradient of boundary. However, weak edge of images cannot be detected because it depends on location of initial curve. The representative model is geodesic active contour model [8], which is improved on the basis of snake model [9]. The edge-based active contour models are sensitive to noise due to local limitation and have difficulty in detecting weak boundary. In recent years, many scholars have put forward various ideas to improve edge-based model. For example, Feng proposed a selective binary Gaussian filter regularization level set (SBGFRLS) method to obtain smoother contour [10]. Khadidos thought that energy terms could be constructed using their relative importance in detecting boundaries [11]. Liu proposed a weighted edge level set method based on multi-local statistics by analyzing the defects of constant length, region coefficient and traditional edge stop function in noise image segmentation [12]. Region-based active contour model uses local information of image to evolve curve. The initial contour can be placed anywhere in the image and if the image information is rich, the internal contour can be detected automatically. The most famous region-based active contour model is the CV model, which assumes that each region of the image is statistically uniform and has been successfully applied to binary phase segmentation [13]. However, since the CV model assumes that the intensity in the foreground and background regions is always constant, this method is not suitable for images with intensity inhomogeneous. Researchers have proposed many methods to overcome the difficulty of image segmentation with intensity inhomogeneous. For instance, Vese et al. and Tsai et al. proposed a piece-by-piece smoothing (PS) model to solve the problem of intensity inhomogeneous images by minimizing MS functional and replacing the piece-by-piece constant intensity with piece-by-piece smoothing intensity [14–16]. These models can deal with the intensity inhomogeneity to some extent, but the calculation cost is high and the segmentation effect is not good. Then, Li et al. constructed a LBF model by adding the kernel function to the variational formula to define the local binary fitting energy, but the model was greatly affected by the initial contour [17]. Zhang et al. proposed a level set method using local image region statistics to segment images with intensity inhomogeneous [18]. Liu and Peng proposed a CV model based on local regions considering local features of images [19]. Wang et al. proposed another LCV model using differential image information [20]. Ma et al. used mean matrix plus variable deviation matrix to fit the non-uniform strength, and this fitting term can approach local intensities more closely [21]. Peng built the Gaussian distribution of each region intensity with spatially varying mean and variance to deal with the images with intensity inhomogeneous [22]. To sum up, it is still challenging to obtain accurate and robust segmentation for image segmentation with intensity inhomogeneous in complex environment.

This paper presents a new medical image segmentation model based on fractional varying-order differential. Firstly, we calculate fractional differential order mask according to image gradient. Then, by using frequency-domain fractional differential we carry out differential operations of different orders for pixel points with different gray values. Finally, adding this mask to the original image, so we can gain a new image pixel characteristic matrix. The local term combined with fractional varying-order differential can describe the original image more accurately and is robust to noise. The length term is used to regularize the image contour length. The penalty term is used to avoid reinitialization [23]. TP rate, FP rate, P rate, JSC and DSC are employed as the comparative measures for the segmented results. The evolution of the level set function results in a gradient flow that minimizes the global energy functional. Experimental results on synthetic images and real images show that this method has good performance.

The rest of this paper is organized as follows. In Section 2, we briefly introduce some related methods. In Section 3, we describe our proposed image segmentation model and in Section 4, we compare the experimental results on real images and synthetic images with other models. The Section 5 discusses the experimental results of the Section 4 and explains them from the perspective of previous studies and working hypotheses. Finally, the conclusion is drawn in Section 6.

2. Materials and Methods

2.1. LBF Model

LBF model can obtain local statistical information by introducing kernel function to solve the shortcoming of CV model based on global information [17]. It can control the mean intensity information as much as possible getting in the vicinity of the pixel. After introducing the level set method, they defined the energy functional as follows:

$$\begin{aligned} E^{LBF}(\phi, f_1, f_2) = \ & \lambda_1 \int [\int K_\sigma(\mathbf{x}-\mathbf{y})|I(\mathbf{y})-f_1(\mathbf{x})|^2 H(\phi(\mathbf{y}))d\mathbf{y}]d\mathbf{x} \\ & +\lambda_2 \int [\int K_\sigma(\mathbf{x}-\mathbf{y})|I(\mathbf{y})-f_2(\mathbf{x})|^2 (1-H(\phi(\mathbf{y})))d\mathbf{y}]d\mathbf{x} \\ & +\mu \int_\Omega \tfrac{1}{2}(|\nabla\phi(\mathbf{x})|-1)^2 d\mathbf{x} + \nu \int_\Omega \delta(\phi(\mathbf{x}))|\nabla\phi(\mathbf{x})|d\mathbf{x} \end{aligned} \tag{1}$$

where $I:\Omega \to \Re^{\mathrm{d}}$ is an image, $\Omega \to \Re^{\mathrm{d}}$ is the image domain, and $d > 1$ is the dimension of this image vector $I(\mathbf{x})$. $\mathbf{x}$ is the center point and $\mathbf{y}$ is the point around $\mathbf{x}$. K_σ is the Gaussian kernel function with standard deviation σ, $\lambda_1 > 0$, $\lambda_2 > 0$, $\mu > 0$ and $\nu > 0$ are fixed parameters. $H(\phi)$ is the Heaviside function. Assuming z is the input of the function, $\delta(z)$ is the Dirac function defined as the derivative of Heaviside function:

$$H(z) = \begin{cases} 1\ , & z \geq 0 \\ 0\ , & z < 0 \end{cases}\ ,\ \delta(z) = \frac{\mathrm{d}}{\mathrm{dz}}H(z) = \begin{cases} 0\ , & z \neq 0 \\ +\infty\ , & z = 0 \end{cases} \tag{2}$$

In practice, the $H(z)$ and $\delta(z)$ can approximated by a smooth function $H_\varepsilon(z)$, $\delta_\varepsilon(z)$:

$$H_\varepsilon(z) = \frac{1}{2}(1+\frac{2}{\pi}\arctan(\frac{z}{\varepsilon})),\ \delta_\varepsilon(z) = \frac{1}{\pi}\frac{\varepsilon}{\varepsilon^2+z^2} \tag{3}$$

Keep the level set function ϕ unchanged, and minimize the energy functional Equation (1) for the local center f_1 and f_2, we can obtain:

$$f_1(\mathbf{x}) = \frac{K_\sigma(\mathbf{x}) * [H_\varepsilon(\phi(\mathbf{x}))\ I(\mathbf{x})]}{K_\sigma(\mathbf{x}) * H_\varepsilon(\phi(\mathbf{x}))}, f_2(\mathbf{x}) = \frac{K_\sigma(\mathbf{x}) * [(1-H_\varepsilon(\phi(\mathbf{x})))\ I(\mathbf{x})]}{K_\sigma(\mathbf{x}) * [1-H_\varepsilon(\phi(\mathbf{x}))]} \tag{4}$$

Although the LBF model can effectively segment inhomogeneous images, it is sensitive to the initial contour.

2.2. LIC Model

According to the LIC model [24], an observed image of the real-world I can be modeled as

$$I = bJ + n \tag{5}$$

where J is the true image, which is an intrinsic physical property of the objects being imaged, thus it can be approximately assumed to be piecewise constant; b is the intensity inhomogeneous component, which is referred to as a bias field (or shading image), and n is additive noise, which can generally be assumed to be zero-mean Gaussian noise. Therefore, they made the true image J approximately take N distinct constant values $c_1, \cdots, c_N$ into disjoint regions $\Omega_1, \cdots, \Omega_N$ and $\{\Omega_i\}_{i=1}^N$ constitutes a partition of the image domain, i.e., $\Omega = \cup_{i=1}^N \Omega_i$ and $\Omega_i \cap \Omega_j = \varnothing$ for $i \neq j$. They defined a circular neighborhood of radius ρ, where each point $\mathbf{y} \in \Omega$ is the center of the circle, defined by $\vartheta_\mathbf{y} \overset{\Delta}{=}: \{\mathbf{x} : |\mathbf{x}-\mathbf{y}| \leq \rho\}$ and the center point $\mathbf{x}$. The partition $\{\Omega_i\}_{i=1}^N$ of the entire domain Ω induces a partition of $\vartheta_\mathbf{y}$. Then, the image model in Equation (5) can be redefined by:

$$I(\mathbf{x}) \approx b(\mathbf{y})c_i \approx b(\mathbf{y})c_i + n(\mathbf{x})\ for\ \mathbf{x} \in \vartheta_\mathbf{y} \cap \Omega_i \tag{6}$$

where $n(\mathbf{x})$ is additive zero-mean Gaussian noise.

Then, the two-phase energy functional after introducing the level set method as follows:

$$\begin{aligned} F(\phi, c, b) &= \int \sum_{i=1}^{N} \left(\int K(\mathbf{y}-\mathbf{x})|I(\mathbf{x}) - b(\mathbf{y})c_i|^2 d\mathbf{y}\right) M_i(\phi(\mathbf{x}))d\mathbf{x} \\ &\quad + \nu \int |\nabla H(\phi)|d\mathbf{x} + \mu \int p(|\nabla\phi|)d\mathbf{x} \end{aligned} \tag{7}$$

where the membership functions defined by:

$$M_1(\phi) = H(\phi), M_2(\phi) = 1 - H(\phi) \tag{8}$$

$\int |\nabla H(\phi)|d\mathbf{x}$ is the length term used to calculate the arc length of the zero level contour of ϕ. $\int p(|\nabla\phi|)d\mathbf{x}$ is the penalty term, which smooths the contour by penalizing the arc length and $p(s) = (1/2)(s-2)^2$ [23].

With respect to c, we can obtain the follow equation:

$$\hat{c}_i = \frac{\int (b * K)Iu_i d\mathbf{y}}{\int (b^2 * K)Iu_i d\mathbf{y}},\ i = 1, \cdots, N \tag{9}$$

with $u_i(\mathbf{y}) = M_i(\phi(\mathbf{y}))$. Equally, with respect to b, we can obtain the follow equation:

$$\hat{b} = \frac{(IJ^{(1)}) * K}{J^{(2)} * K} \tag{10}$$

where $J^{(1)} = \sum_{i=1}^{N} c_i u_i$ and $J^{(2)} = \sum_{i=1}^{N} c_i^2 u_i$.

This model can segment images with intensity inhomogeneous and more robust to contour initialization. Moreover, this model is much more efficient than the LBF model.

2.3. The Fractional Order Differential

The commonly used definitions of fractional derivatives include: Grünwald–Letnikov derivative, Riemman–Liouville fractional derivative, Caputo fractional derivative, Laplace-domain fractional derivative, frequency-domain (Fourier domain) fractional derivative. As the fast discrete Fourier transform is easy to calculate numerically, fractional derivatives in frequency domain are used in this paper.

For a given function of a single variable $g(t)$, its Fourier transform can be defined as:

$$G(\omega) = \int_R g(t)e^{-j\omega t}dt \tag{11}$$

where j is the imaginary number, t is the time variable, ω is the frequency variable, $g(t)$ is the original function, and the function $G(\omega)$ is called the image function of the Fourier transform. Using the differential properties of the Fourier transform, compute the n−th derivative:

$$F(g^n(t)) = (j\omega)^n G(\omega) \tag{12}$$

where n is a non-negative integer, F is the Fourier transform operator. The Fourier domain expression for any order differential can be obtained directly:

$$D^\alpha g(t) = F^{-1}(\ (j\omega)^\alpha G(\omega)),\ \alpha \in \Re^+ \tag{13}$$

where $\Re^+$ is the set of positive real number, α is a positive real number and F^{-1} is the inverse Fourier transform operator. Thus, the fractional order partial differential of the two-dimensional function $g(x, y)$ can be defined as follows:

$$\begin{cases} D_x^\alpha g(x,y) = F^{-1}((j\omega_1)^\alpha G(\omega_1, \omega_2)) \\ D_y^\alpha g(x,y) = F^{-1}((j\omega_2)^\alpha G(\omega_1, \omega_2)) \end{cases} \tag{14}$$

where $G(\omega_1, \omega_2)$ is the Fourier transform of $g(x, y)$. D_x^α means the α-th order differential of the variable x.

By using the translation property of two-dimensional DFT, the central difference scheme of the first order derivative in Fourier domain is obtained:

$$\begin{cases} D_x^\alpha g(x,y) = F^{-1}((1-\exp(-2\pi j\omega_1/m)^\alpha \exp(\pi j\alpha\omega_1/m)G(\omega_1,\omega_2)) \\ D_y^\alpha g(x,y) = F^{-1}((1-\exp(-2\pi j\omega_2/m)^\alpha \exp(\pi j\alpha\omega_2/m)G(\omega_1,\omega_2)) \end{cases} \tag{15}$$

The fractional order differential has the characteristics of increasing the high frequency component of the signal while preserving the low frequency component of the signal nonlinearly. Therefore, fractional order differential has gained more and more attention and application in the field of image processing. At present, the fractional order differential operation in image processing is performing the same-order differential operation on the whole image, which is inconsistent with the characteristics of different pixel values in different texture details of the image, so the texture details are partially damaged or smoothed out when the image is performed same-order differential operation, which will seriously affect the quality of the image and its effect on further analysis and understanding.

3. The Proposed Model

The traditional image processing methods based on fractional order differential use a constant-order differential, in other word, it is the same differential order for a whole image. Due to the characteristics of the pixel values, the actual image has different texture details in different parts. When the same order fractional order differential operation was carried out on the whole image, some parts of the texture that should not be processed at this order will be damaged or smoothed, seriously affecting the quality of image. It will influence the further analysis and understanding. Therefore, we hope to use an operation to make pixels at different positions carry out differential order operations according to their own characteristics. We will use the matrix structure of a new fractional order differential operator, allows us to apply different differential order to the different parts of image, then we can get a more detailed image information so that we can process it conveniently.

3.1. Fractional Varying-Order Differential

Supposing $u(x, y)$ is a two-dimensional image, firstly we calculate the gradient information of the image, because the edge of the image exists in the gradient information. Then, we suppose A is a $n \times m$ matrix, and its value is obtained by the following operation after obtaining the image gradient information:

$$A = a \cdot \frac{(|\nabla u| + 1)}{|\nabla u| + 0.8} \tag{16}$$

where a is adapting weight, we defined:

$$a = \begin{cases} 4 & gray\ value \geq 130 \\ 0.0001 & gray\ value < 130 \end{cases} \tag{17}$$

The order of fractional differential can be adaptively adjusted according to the local statistical information and structural characteristics of the image, so that it can be satisfied that it has a large differential order at the strong edge of the image, and a small differential order at the weak edge and texture of the image. In this paper, the value of a is the optimal value obtained through experimental tests. We regard A as the order matrix calculated from the image gradient. Additionally, then the fractional order differential operation is carried out according to the order matrix. The fractional varying-order differential operator with different orders of each pixel point is obtained by:

$$D_A = \begin{pmatrix} D_{A_{11}} & D_{A_{12}} & \cdots & D_{A_{1m}} \\ D_{A_{21}} & D_{A_{22}} & \cdots & D_{A_{2m}} \\ \vdots & \vdots & \ddots & \vdots \\ D_{A_{n1}} & D_{A_{n2}} & \cdots & D_{A_{nm}} \end{pmatrix} \tag{18}$$

thus, the corresponding fractional varying-order partial derivatives are

$$\begin{cases} D_{Ax}u(x,y) = F^{-1}(j\omega_1)^A U(\omega_1,\omega_2) \\ D_{Ay}u(x,y) = F^{-1}(j\omega_2)^A U(\omega_1,\omega_2) \end{cases} \tag{19}$$

the corresponding A-order differential of image u can be updated to:

$$D_A u = (D_{Ax}u, D_{Ay}u), \qquad |D_A u| = |D_{Ax}u| + |D_{Ay}u| \tag{20}$$

As fractional derivative is a linear operator, the modulus value obtained after square and extraction of square root is obviously not linear, but the linear change of gray scale can be retained after absolute value operation, so the absolute value is used instead of the square operation.

3.2. Energy Formulation

The energy functional in our proposed model mainly consists of three parts: the local term E^L, the length (or regulation) term E^R, and the penalty term E^P. The local term combined with the fractional varying-order differential to gain more image information. For a given image vector $u(\mathbf{x})$, $\mathbf{x}$ is a two dimensional vector, represented by $\mathbf{x}(x,y)$. The fractional varying-order gradient magnitude is defined by:

$$mag(D_A u(\mathbf{x})) = |D_{Ax}u| + |D_{Ay}u| \tag{21}$$

then a new difference image $I(\mathbf{x})$ is constructed:

$$I(\mathbf{x}) = u(\mathbf{x}) + mag(D_A u(\mathbf{x})) \tag{22}$$

finally, the proposed local energy fitting is defined as follows:

$$E^L = \int (\sum_{i=1}^{N} \int K(\mathbf{y}-\mathbf{x})|I(\mathbf{x}) - b(\mathbf{y})c_i|^2 d\mathbf{x}) d\mathbf{y} \tag{23}$$

when the image domain Ω is divided into two disjoint regions Ω_1 and Ω_2, the two regions are represented by the level set function ϕ:

$$\Omega_1 = \{\mathbf{x} : \phi(\mathbf{x}) \geq 0\},\ \Omega_2 = \{\mathbf{x} : \phi(\mathbf{x}) < 0\} \tag{24}$$

the regions Ω_1 and Ω_2 can be represented by the membership function defined in Equation (8). Thus, for the two-phase case, the energy in Equation (23) can be expressed as the following level set formulation:

$$\begin{aligned} E^L(\phi, c, b) &= \int (\sum_{i=1}^{N} \int K(\mathbf{y}-\mathbf{x})|I(\mathbf{x}) - b(\mathbf{y})c_i|^2 M_i(\phi(\mathbf{x})) d\mathbf{x}) d\mathbf{y} \\ &= \int \sum_{i=1}^{N} (\int K(\mathbf{y}-\mathbf{x})|I(\mathbf{x}) - b(\mathbf{y})c_i|^2 d\mathbf{y}) M_i(\phi(\mathbf{x})) d\mathbf{x} \end{aligned} \tag{25}$$

for fixed ϕ and b, we can still get Equations (9) and (10).

In the three-phase case, we can use:

$$\begin{aligned} M_1(\phi_1, \phi_2) &= H(\phi_1)H(\phi_2) \\ M_1(\phi_1, \phi_2) &= H(\phi_1)(1 - H(\phi_2)) \\ M_1(\phi_1, \phi_2) &= 1 - H(\phi_1) \end{aligned} \tag{26}$$

The proposed local term has two features. Firstly, the fractional order differential has good performance in preserving and enhancing low frequency information and we use matrix operation to apply diverse differential orders to the different parts of the image. Thus, we can gain more detailed image information and improve the performance of segmenting intensity inhomogeneous images. Secondly, the fractional order differential has a filtering effect. After fractional order differential operation, the image is smoother than the original image, and the contrast is also improved, therefore, the noise immunity can be improved to a certain extent, and more accurate segmentation results can be obtained effectively.

E^R and E^P are the same with the LIC model:

$$E^R = \int |\nabla H(\phi)| d\mathbf{x},\ E^P = \int p(|\nabla \phi|) d\mathbf{x} \tag{27}$$

The final energy functional can be described as:

$$\begin{aligned} E &= E^L + \nu E^R + \mu E^P \\ &= \int \sum_{i=1}^{N} \left(\int K(\mathbf{y}-\mathbf{x})|I(\mathbf{x}) - b(\mathbf{y})c_i|^2 d\mathbf{y}\right) M_i(\phi(\mathbf{x})) d\mathbf{x} \\ &+ \nu \int |\nabla H(\phi)| d\mathbf{x} + \mu \int p(|\nabla \phi|) d\mathbf{x} \end{aligned} \tag{28}$$

defining $e_i(\mathbf{x}) = \int K(\mathbf{y}-\mathbf{x})|I(\mathbf{x}) - b(\mathbf{y})c_i|^2 d\mathbf{y}$ and utilizing variational strategy to minimize the energy functional, the corresponding energy functional gradient descent flow can be obtained:

$$\frac{\partial \phi}{\partial t} = -\frac{\partial E}{\partial \phi} = -\delta(\phi)(e_1 - e_2) + \nu\delta(\phi) div \frac{\nabla(\phi)}{|\nabla \phi|} + \mu(div(d_p(|\nabla \phi|))\nabla(\phi)) \tag{29}$$

where $\frac{\partial E}{\partial \phi}$ is the Gâteaux derivative [25], ∇ is the gradient operator, $div()$ represents the divergence operator, and the function d_p is:

$$d_p(s) = \frac{p'(s)}{s} \tag{30}$$

Gradient descent flow of the multiphase energy functional are:

$$\begin{aligned} \frac{\partial \phi_1}{\partial t} &= -\sum_{i=1}^{N} \frac{\partial M_i(\phi)}{\partial \phi_1} e_i + \nu\delta(\phi_1) div \frac{\nabla(\phi_1)}{|\nabla \phi_1|} + \mu(div(d_p(|\nabla \phi_1|))\nabla(\phi_1)) \\ &\vdots \\ \frac{\partial \phi_k}{\partial t} &= -\sum_{i=1}^{N} \frac{\partial M_i(\phi)}{\partial \phi_k} e_i + \nu\delta(\phi_k) div \frac{\nabla(\phi_k)}{|\nabla \phi_k|} + \mu(div(d_p(|\nabla \phi_k|))\nabla(\phi_k)) \end{aligned} \tag{31}$$

3.3. Implementation and Algorithm

The implementation and algorithm of this model consists of the following steps:

1. Set up the initial required parameter value and iteration number, calculate fractional order differential order mask according to image gradient and add it to the original image.
2. Initialize the level set function ϕ to a function ϕ_0 (ϕ_0 is the initialize level set function). Then, construct the initial contour C.
3. Update $\phi_{i,j}^{k+1} = \phi_{i,j}^{k} + \Delta t \cdot A(u_{ij}^k)$, where $A(u_{ij}^k)$ is the right side of the Equation (29).

4. Update $\hat{c}_i$, $\hat{b}_i$ by Equations (9) and (10).
5. Check if the set number of iterations is reached. If not, return to step 2.

4. Results

In this section, we have carried out various experiments of synthetic and real image segmentation of different types of contours and shapes. We also compare results of our model with the CV model, the LBF model, the LIC model, the ALFB model [21] and fractional order differentials with fixed orders of 1.5 and 0.5. In addition, we use TP rate, FP rate, P rate, JSC, and DSC to measure the pros and cons of the image segmentation results, which defined by:

$$\begin{gathered} DSC = \frac{2(S_1 \cap S_2)}{S_1 + S_2}, TP = \frac{|S_1 \cap S_2|}{|S_2|}, FP = \frac{|S_1 \cap S_2 - S_2|}{|S_2|} P = \frac{TP}{TP+FP} \\ , JSC = \frac{|S_1 \cap S_2|}{|S_1 \cup S_2|} \end{gathered} \tag{32}$$

where S_1 and S_2 represent the output binary image and ground binary image after segmentation, respectively. The value of ground truth is obtained by selecting the appropriate threshold through the imbinarize function in the MATLAB software. The closer the values of DSC, TP, P and JSC are to 1, and the values of FP is to 0, the better the segmentation effect. All the experiments are carried out by Matlab(R2017b) in a Lenovo laptop with an Intel(R) Core (TM) i3-4030U CPU @ 1.90GHz processer. The parameters are set as follows: $\lambda_1 = \lambda_2 = 1$, $\nu = 0.001 \times 255^2$, $\mu = 1$, $\Delta t = 0.1$ (the time step), The default value of σ is 10, and the default value of the initial contour is [40:100, 50:100] (Except for Section 4.1). In the following experiments, we will also prove whether our model is affected by the value of σ and the initial contour.

4.1. Performance on Different Initial Contours

Firstly, we apply our method to an image to quantitatively evaluate the performance of our method under different initial contours. We set 20 different initial contours to obtain the corresponding experimental data. Figure 1 shows any 5 segmentation results of these 20 different initial contours, we can see that these different initial contours can finally capture the boundary of the objects from these figures. It confirms that our model cannot be affected by different initial contours. Figure 2 shows the evaluation index values corresponding to 20 different initial contour segmentation results.

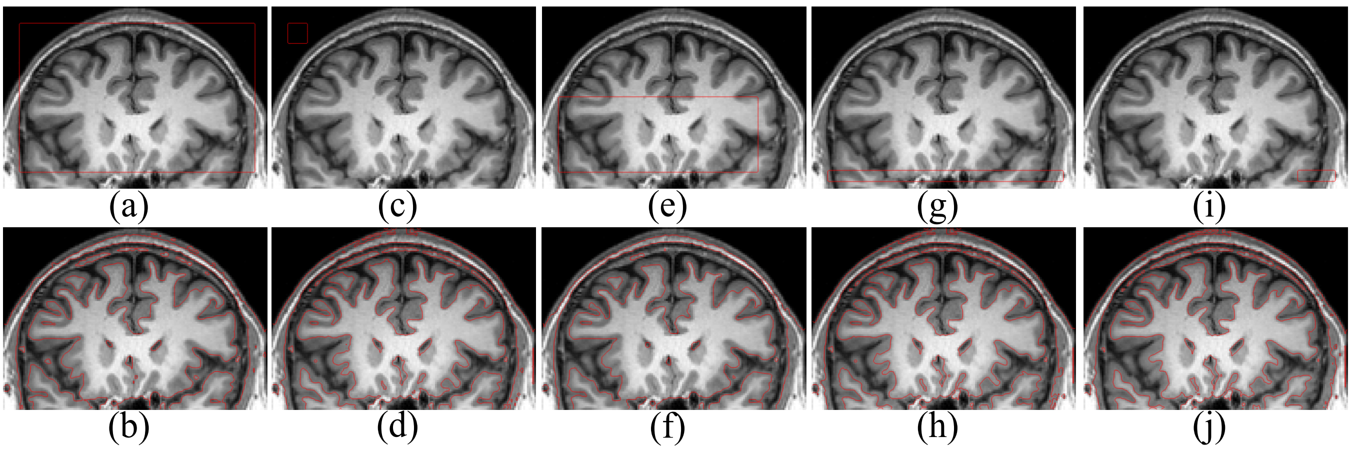

Figure 1. Segmentation results of our model with 5 different initial contours. (**a**) original image with initial contours; (**b**) the corresponding segmentation results of (**a**); (**c**) original image with initial contours, (**d**) the corresponding segmentation results of (**c**); (**e**) original image with initial contours; (**f**) the corresponding segmentation results of (**e**); (**g**) original image with initial contours; (**h**) the corresponding segmentation results of (**g**); (**i**) original image with initial contours; (**j**) the corresponding segmentation results of (**i**).

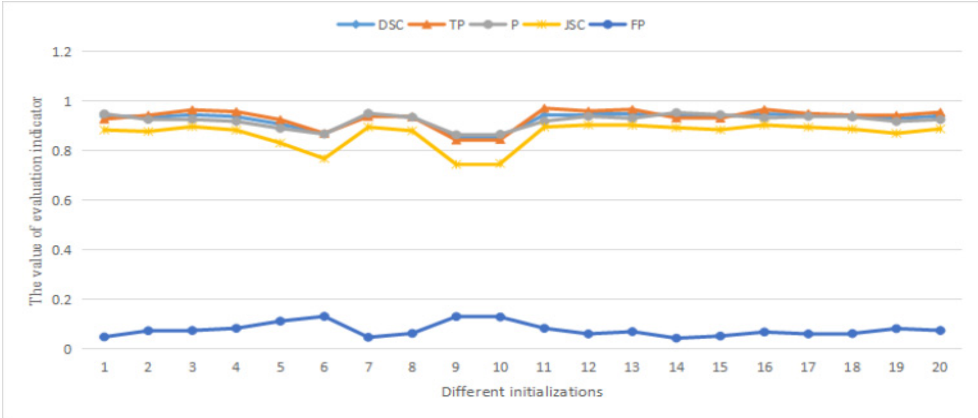

Figure 2. The corresponding evaluation index values of 20 different initial contours.

4.2. Performance under Different Levels of Noise

Next, in order to prove that our segmentation results are more robust, we use our model on Figure 3 to segment images under different noise conditions and compare with the CV model, the LBF model, the LIC model, and fractional order differentials with fixed orders of 1.5 and 0.5. We use MATLAB's imnoise function to obtain two kinds of noise with variance values of 0.01 and 0.02, respectively. The variance noise of the first row is 0.01, and the noise of the second row is 0.02. It can be seen from Figure 3e,g that the added noise with a variance of 0.01 has a bad influence on the LBF model and the 0.5-order segmentation results. For the LIC model (see Figure 3c,d), the addition of noise with a variance of 0.01 has a slight impact on the segmentation results, but the addition of noise with a variance of 0.02 has a very obvious impact on the segmentation results. When the fractional order is 1.5 (see Figure 3i,j), adding noise with variance of 0.01 has an impact on the internal segmentation results of the image, and adding noise with variance of 0.02 has more effect on the segmentation result than other models. Compared with other models, our model can withstand part of the influence of noise and obtain better segmentation results.

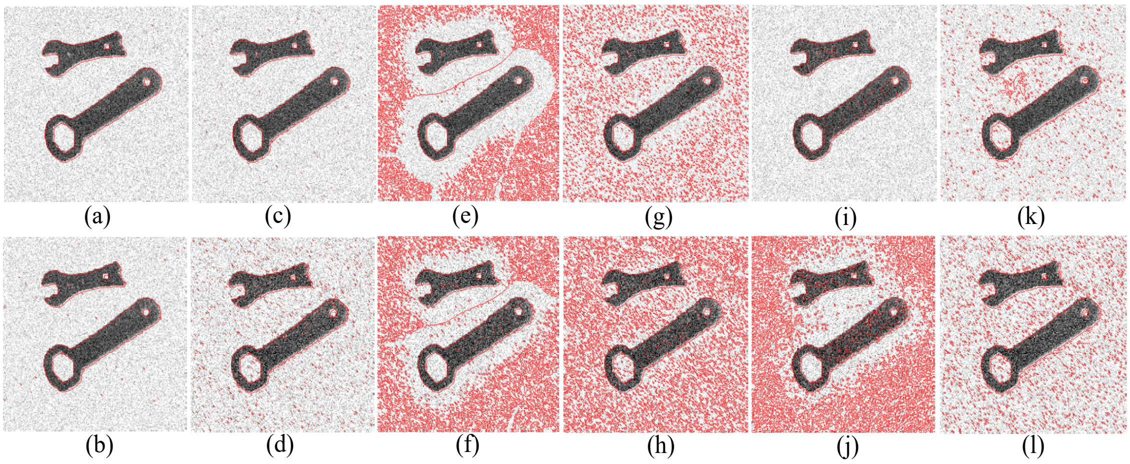

Figure 3. Segmentation results after adding noise. (**a**) The result of adding noise with variance of 0.01 to our model; (**b**) the result of adding noise with variance of 0.02 to our model; (**c**) the results of adding noise with variance of 0.01 to LIC model; (**d**) the results of adding noise with variance of 0.02 to LIC model; (**e**) the results of adding noise with variance of 0.01 to LBF model; (**f**) the results of adding noise with variance of 0.02 to LBF model; (**g**) the results of adding noise with variance of 0.01 to 0.5-order; (**h**) the results of adding noise with variance of 0.02 to 0.5-order; (**i**) the results of adding noise with variance of 0.01 to 1.5-order; (**j**) the results of adding noise with variance of 0.02 to 1.5-order; (**k**) the results of adding noise with variance of 0.01 to CV model; and (**l**) the results of adding noise with variance of 0.02 to CV model.

4.3. Performance on Different Images and Comparison with Other Models

We demonstrated the effectiveness of our model by comparing the segmentation results of our model with the CV model, LBF model, LIC model, ALFB model and fixed-order differential (see Figures 4–6). In the figure, (a–c) are the original image, the original image with the initial contour and the ground truth of the original image, respectively. (d–f) are the segmentation results of our model, (g–i) are the segmentation results of LIC model, (j–l) are the segmentation results of LBF model, (m–o) are the segmentation results of 0.5-order fractional order differential, (p–r) are the segmentation results of 1.5-order fractional order differential, (s–u) are the segmentation results of CV model, and (v–x) are the segmentation results of ALFB model. The figure also shows the comparison map of segmented regions (the red area represents the part that should be segmented compared with the ground truth of the original image, but the actual result is not segmented, and the green area represents the actual segmentation, but the part that should not be segmented is compared with the ground truth of the original image) and the ground truth image of the final segmentation result. The advantages of our model can be seen from the evaluation index values of the segmentation results corresponding to each graph (see Table 1). In addition, in order to further compare the two models, different σ values are also set for comparison (see Figure 7).

Table 1. The corresponding evaluation index values of Figure 4.

	Our	**LIC**	**LBF**	**0.5-Order**	**1.5-Order**	**CV**	**ALFB**
DSC	**0.9665**	0.9532	0.8941	0.8326	0.8716	0.9463	0.5465
TP	0.9889	0.9917	0.8654	0.7227	0.8366	**1**	0.3760
FP	0.0575	0.0892	0.0704	0.0132	0.0831	0.1135	$\mathbf{1.7575 \times 1^{-4}}$
P	0.9450	0.9175	0.9248	0.9821	0.9096	0.8981	**0.9995**
JCS	**0.9351**	0.9105	0.8085	0.7133	0.7724	0.8981	0.3760

4.4. Performance on Abdominal CT Image

At the same time, we used abdominal CT images taken by one of the authors of this paper during a hospital physical examination this year to compare the actual effectiveness of these segmentation models, as shown in Figure 8. It can be clearly seen from (g) in Figure 8 that the CV model cannot recognize the edge of the image because the initial contour we set is far from the image. As can be seen from (c–f) in Figure 8, unnecessary contours appear in the segmentation results of other models. However, our model still maintains a good segmentation effect, which reflects the advantages of our model.

4.5. Performance on Multiphase Level Set Function

Finally, compared with the LIC model and the ALFB model, we tested the multiphase level set function of the brain image (see Figures 9–11). We can see from Figure 9f,g, Figure 10f,g and Figure 11f,g that the segmentation effect of the ALFB model is far inferior to our model and the LIC model. Compared with the LIC model, our model is very sensitive to the change of the image gray value. We can see that the red area in the figure is obviously more than that of the LIC model, and the blue area also includes the areas not recognized by the LIC model in some details. In addition, in the LIC paper, it is introduced that whether the image quality is improved through comparing the original image and the histogram of the bias correction image [24]. Due to the mixing of the intensity distribution caused by the deviation, the original image cannot have well-separated peaks. However, the histogram of our model (see Figures 9h, 10h and 11h) shows three well-separated peaks on the histogram of the image after deviation-correction, which correspond to the target or background of the image.

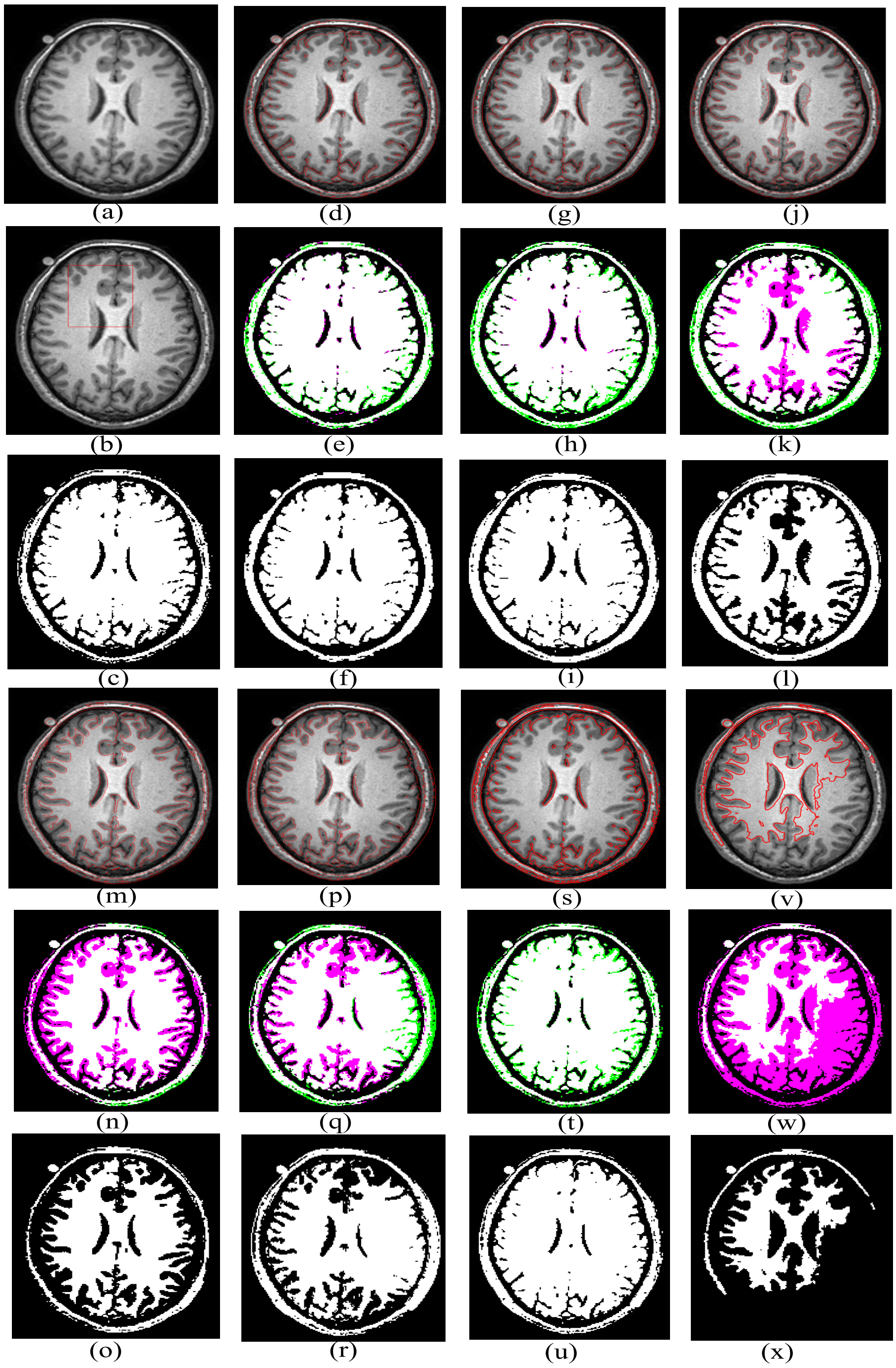

Figure 4. Performance of our method, the LIC model, the LBF model, 0.5-order, 1.5-order, the CV model and the ALFB model. (**a**) Original image; (**b**) the original image with the initial contour; (**c**) the ground truth of the original image; (**d**) the segmentation result of our method; (**e**) the comparison map of our method; (**f**) the ground truth of our method; (**g**) the segmentation result of LIC model; (**h**) the comparison map of LIC model; (**i**) the ground truth of LIC model; (**j**) the segmentation result of LBF model; (**k**) the comparison map of LBF model; (**l**) the ground truth of LBF model; (**m**) the segmentation result of 0.5-order; (**n**) the comparison map of 0.5-order; (**o**) the ground truth of 0.5-order; (**p**) the segmentation result of 1.5-order; (**q**) the comparison map of 1.5-order; (**r**) the ground truth of 1.5-order; (**s**) the segmentation result of CV model; (**t**) the comparison map of CV model; (**u**) the ground truth of CV model; (**v**) the segmentation result of ALFB model; (**w**) the comparison map of ALFB model; and (**x**) the ground truth of ALFB model.

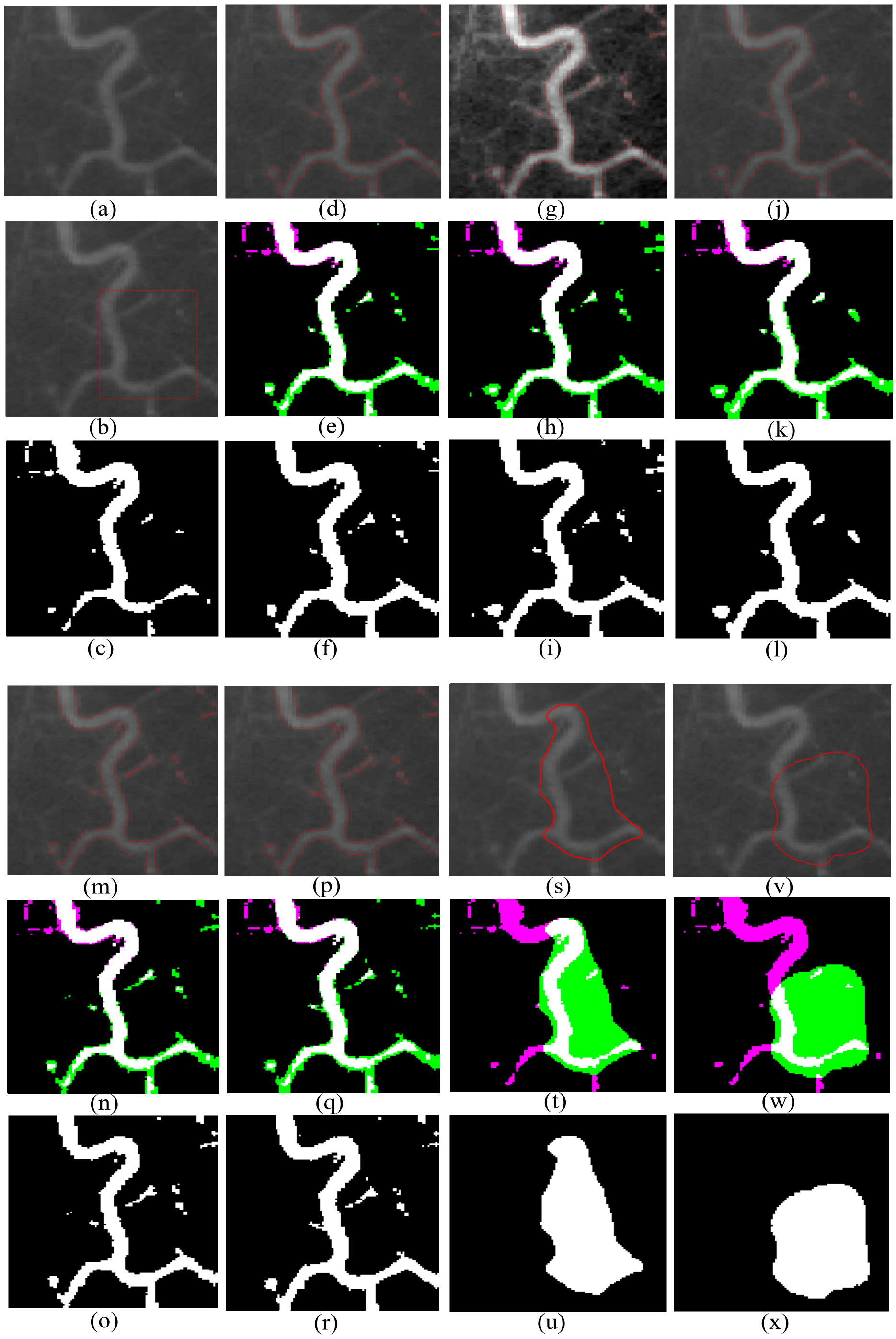

Figure 5. Performance of our method, the LIC model, the LBF model, 0.5-order, 1.5-order, the CV model and the ALFB model. (**a**) Original image; (**b**) the original image with the initial contour; (**c**) the ground truth of the original image; (**d**) the segmentation result of our method; (**e**) the comparison map of our method; (**f**) the ground truth of our method; (**g**) the segmentation result of LIC model; (**h**) the comparison map of LIC model; (**i**) the ground truth of LIC model; (**j**) the segmentation result of LBF model; (**k**) the comparison map of LBF model; (**l**) the ground truth of LBF model; (**m**) the segmentation result of 0.5-order; (**n**) the comparison map of 0.5-order; (**o**) the ground truth of 0.5-order; (**p**) the segmentation result of 1.5-order; (**q**) the comparison map of 1.5-order; (**r**) the ground truth of 1.5-order; (**s**) the segmentation result of CV model; (**t**) the comparison map of CV model; (**u**) the ground truth of CV model; (**v**) the segmentation result of ALFB model; (**w**) the comparison map of ALFB model; and (**x**) the ground truth of ALFB model.

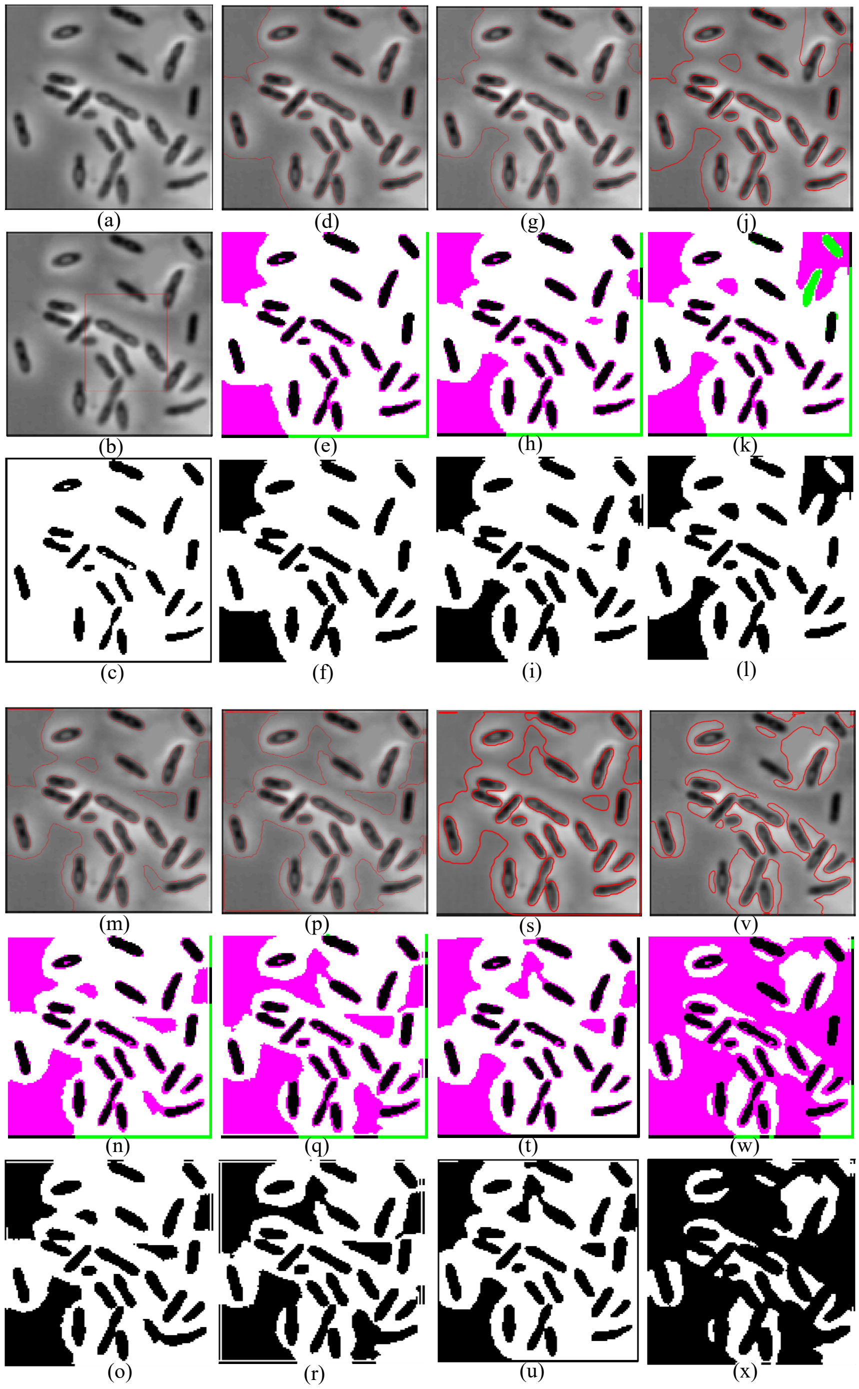

Figure 6. Performance of our method, the LIC model, the LBF model, 0.5-order, 1.5-order, the CV model and the ALFB model. (**a**) Original image; (**b**) the original image with the initial contour; (**c**) the ground truth of the original image; (**d**) the segmentation result of our method; (**e**) the comparison map of our method; (**f**) the ground truth of our method; (**g**) the segmentation result of LIC model; (**h**) the comparison map of LIC model; (**i**) the ground truth of LIC model; (**j**) the segmentation result of LBF model; (**k**) the comparison map of LBF model; (**l**) the ground truth of LBF model; (**m**) the segmentation result of 0.5-order; (**n**) the comparison map of 0.5-order; (**o**) the ground truth of 0.5-order; (**p**) the segmentation result of 1.5-order; (**q**) the comparison map of 1.5-order; (**r**) the ground truth of 1.5-order; (**s**) the segmentation result of CV model; (**t**) the comparison map of CV model; (**u**) the ground truth of CV model; (**v**) the segmentation result of ALFB model; (**w**) the comparison map of ALFB model; and (**x**) the ground truth of ALFB model.

Figure 7. The corresponding evaluation index values of Figure 4 and comparison with the LIC model evaluation index values. (**a**) DSC values; (**b**) P values; (**c**) JSC values; (**d**) TP values; (**e**) FP values; and (**f**) CPU time values.

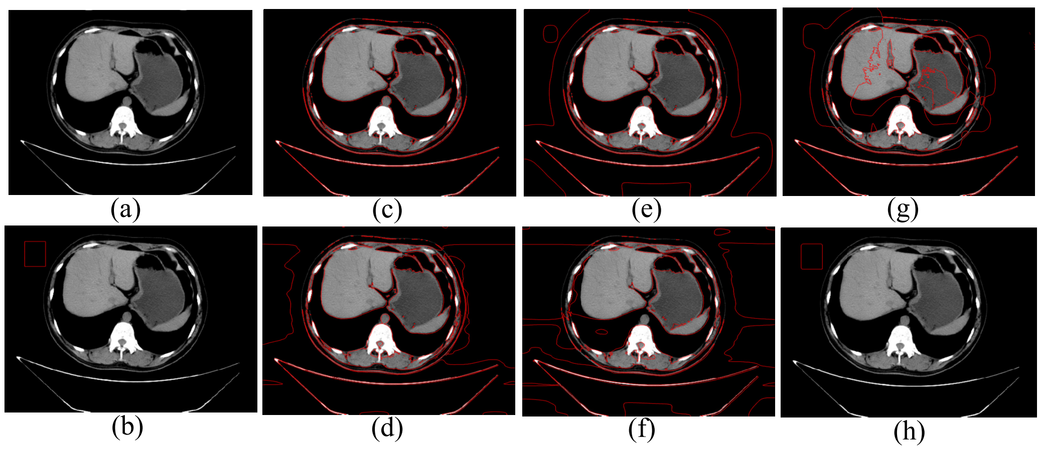

Figure 8. Performance of our method, the LIC model, the LBF model, 0.5-order, 1.5-order on skeleton CT image, and the CV model. (**a**) Original image; (**b**) original image with initial contour; (**c**) the results of our model; (**d**) the results of 0.5 order; (**e**) the results of LIC model; (**f**) the results of 1.5-order; (**g**) the results of LBF model; and (**h**) the results of CV model.

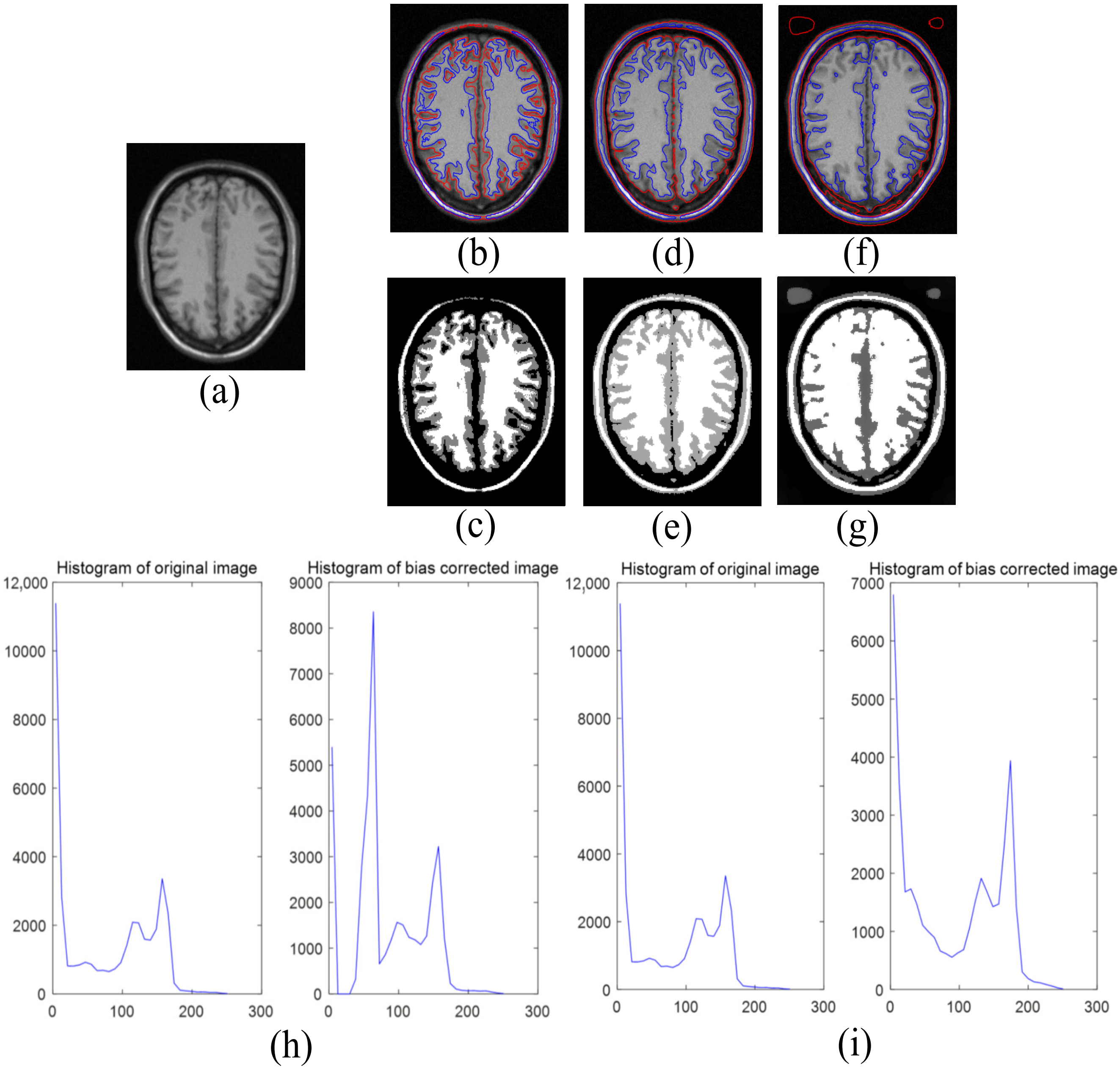

Figure 9. Performance of multiphase level set function and compared with the LIC model and the ALFB model. (**a**) Original image; (**b**) the results of our model; (**c**) the ground truth of our model; (**d**) the result of LIC model; (**e**) the ground truth of LIC model; (**f**) the result of ALFB model; (**g**) the ground truth of ALFB model; (**h**) the histogram of the original image and our model; and (**i**) the histogram of the original image and LIC model.

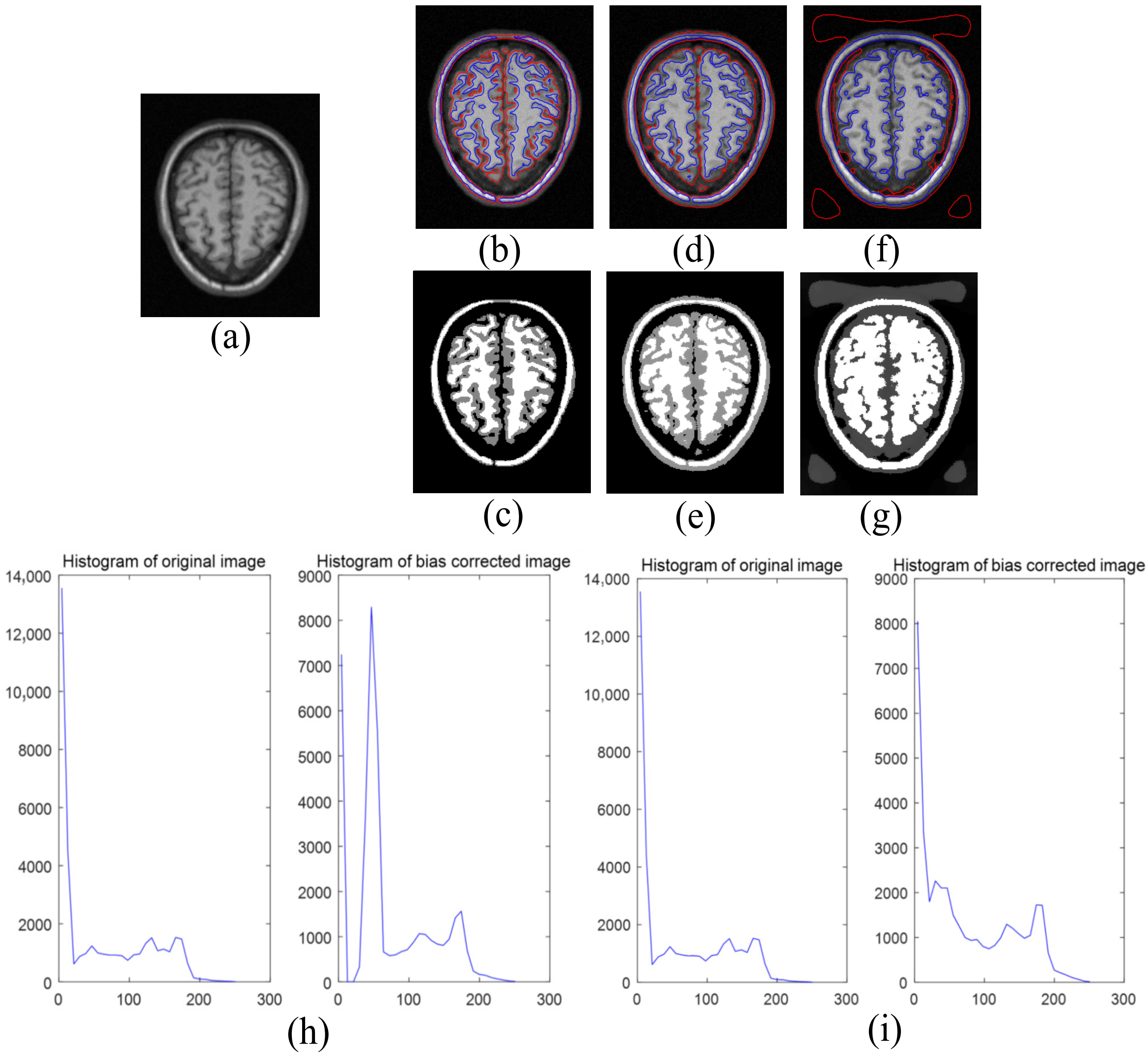

Figure 10. Performance of multiphase level set function and compared with the LIC model and the ALFB model. (**a**) Original image; (**b**) the results of our model; (**c**) the ground truth of our model; (**d**) the result of LIC model; (**e**) the ground truth of LIC model; (**f**) the result of ALFB model; (**g**) the ground truth of ALFB model; (**h**) the histogram of the original image and our model; and (**i**) the histogram of the original image and LIC model.

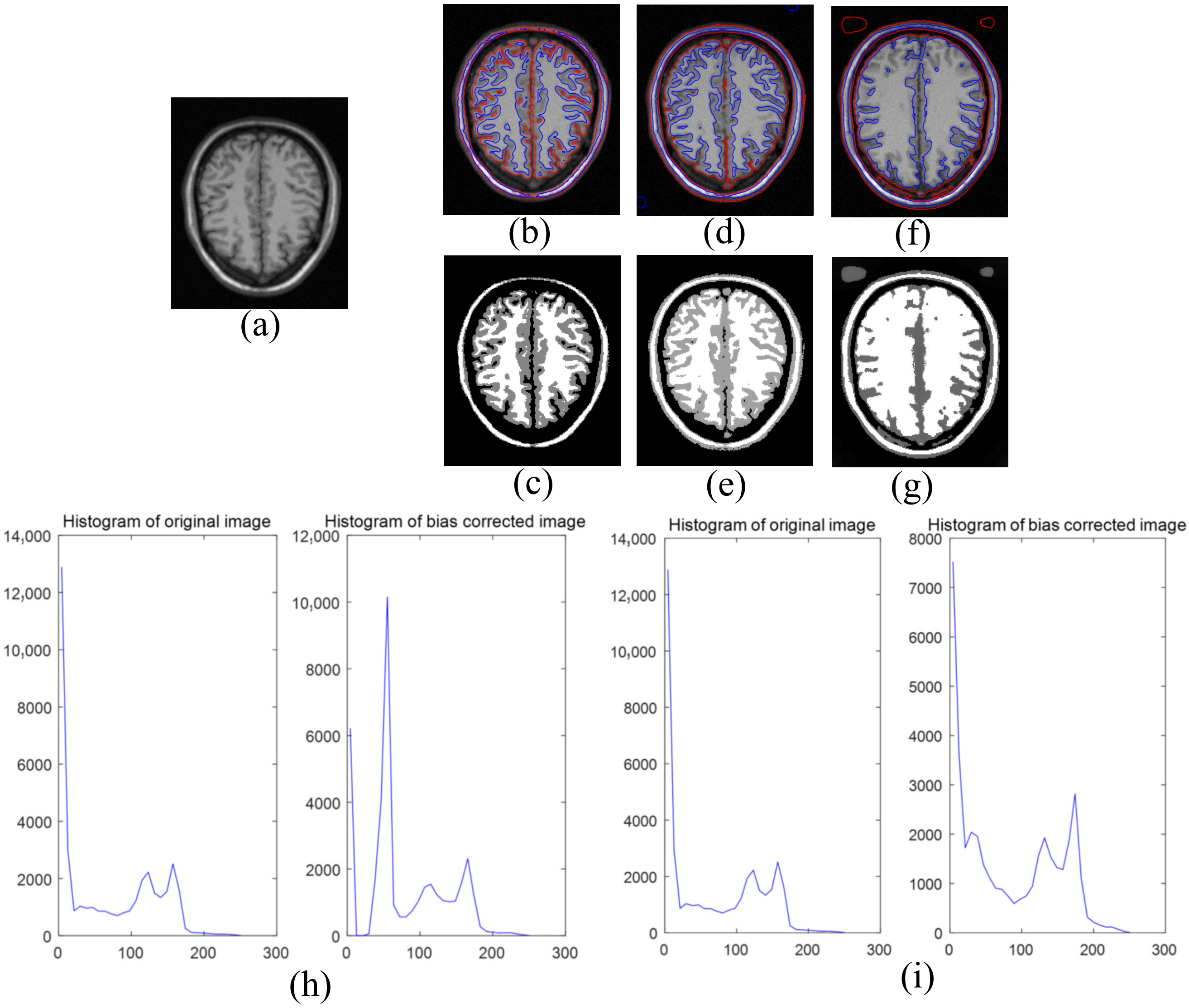

Figure 11. Performance of multiphase level set function and compared with the LIC model and the ALFB model. (**a**) Original image; (**b**) the results of our model; (**c**) the ground truth of our model; (**d**) the result of LIC model; (**e**) the ground truth of LIC model; (**f**) the result of ALFB model; (**g**) the ground truth of ALFB model; (**h**) the histogram of the original image and our model; and (**i**) the histogram of the original image and LIC model.

5. Discussion

The first experiment shows the performance of our model under different initial contours. It has been proved that our model is not affected by the initial contour. TP represents the number of positive classes that are correctly predicted to be positive, and FP represents the number of negative classes that are incorrectly predicted to be positive. From the corresponding values of TP and FP in Figure 2 when the abscissa is 7 or 11, it can be seen that as the number of positive classes correctly predicted as positive classes increases, as the number of negative classes are incorrectly predicted as positive classes decreases, the value of P will increase; however, from the corresponding values of TP and FP in Figure 2 when the abscissa is 9–10, as the number of positive classes correctly predicted as positive classes decreases, as the number of negative classes are incorrectly predicted as positive classes decreases, the value of P will also increase. In addition, we can see that the overall trend of DSC, P and JSC remains the same, and the change of JSC is greater than that of DSC and P, indicating that JSC is more sensitive to changes in pixel set classification than DSC and P.

From the segmentation results of the CV model in Figures 4 and 6, it can be seen that the CV model, as a classic image algorithm, can segment most regions, but the processing of contour edges is very rough actually, and many details are not separated. In the segmentation result of Figure 5, the CV model cannot segment the image because the gray values are too close. This shows that the CV model cannot segment intensity inhomogeneous images. The LBF model is easily affected by level set initialization. In the experiment, the segmentation result obtained by the initial value of the initial contour set by us is not bad, and the difference from other models is mainly reflected in the evaluation index. From Tables 1–3, we can clearly see that the evaluation index of the segmentation result of the LBF model is significantly lower than our model. As we have added the fractional varying-order differential on the basis of the LIC model, inheriting the good characteristics of the LIC model, and at the same time playing the advantages of the fractional varying-order differential, we are more careful in processing the details of the image. We can see it from the evaluation index of Tables 1–3.

Table 2. The corresponding evaluation index values of Figure 5.

	Our	**LIC**	**LBF**	**0.5-Order**	**1.5-Order**	**CV**	**ALFB**
DSC	**0.8227**	0.8014	0.8103	0.8114	0.8065	0.4533	0.2373
TP	0.9208	0.912	0.9167	0.906	**0.9308**	0.6279	0.3298
FP	0.3177	0.364	0.3459	0.3271	0.3774	1.1424	**1.45**
P	**0.7435**	0.7147	0.7261	0.7347	0.7115	0.3547	0.1853
JCS	**0.6988**	0.6686	0.6811	0.6827	0.6758	0.2931	0.1346

Table 3. The corresponding evaluation index values of Figure 6.

	Our	**LIC**	**LBF**	**0.5-Order**	**1.5-Order**	**CV**	**ALFB**
DSC	**0.8819**	0.8583	0.8316	0.8218	0.7460	0.8346	0.4426
TP	**0.8082**	0.7691	0.7399	0.7131	0.6059	0.7162	0.2864
FP	0.0246	0.023	0.0397	0.0225	0.0186	**0**	0.0081
P	0.9704	0.971	0.9491	0.9694	0.9702	**1**	0.9726
JCS	**0.7888**	0.7518	0.7117	0.6974	0.5948	0.7162	0.2842

As can be seen from the line chart of different indicators in Figure 7, our model is superior to the LIC model in the values of four evaluation indicators DSC, FP, JCS, and FP. In terms of TP evaluation indicators, our model is better than the LIC model at first, and LIC is better than our model after the σ value is equal to 8, but the difference between them is not more than 0.01. From the time required for algorithm iteration, see Figure 7d, the CPU time increases as the value of σ increases. In the case of different σ values, after our model undergoes the action of fractional varying order differential, the CPU time required by the LIC model is basically the same, indicating that our model does not consume too much algorithm iteration time. Judging from the 0.5-order and 1.5-order segmentation results, the effect of using the same-order differential on the entire image is not as good as the varying-order differential. The ALFB model uses the mean matrix to add a variable deviation matrix to fit the inhomogeneous intensity. In experiments, we found that this model is very dependent on the initial contour. The initial contour must enclose a large area of the image to segment the target, and the convergence speed is extremely slow, which easily leads to segmentation failure. In order to see the segmentation effect more clearly, we divide the segmented image into a red-green contrast image and a binary image according to the contour. As we use fractional derivatives of different orders in different intensity parts, we can clearly see that our model can achieve finer edge contours than other models compared with ground truth images. Our model can still distinguish regions with very similar gray values in the image. For the expandable gray areas formed in the sulci and gyrus in Figure 4, our method shows good robustness in processing these areas. We can see that the edges are finer than these models and can handle some details better. At the same time, it can also reflect the superiority of our model in evaluating index values.

6. Conclusions

In this paper, we proposed a new method that incorporated fractional varying-order differential and local fitting energy to construct a new variational level set active contour model. We introduced an adapting weight a about image gradient information to get diverse fractional orders. Application of fractional varying-order differential allows us to have more details about the images, so our segmentation result is more delicate and closer to the image boundary, so our model can segment images with intensity inhomogeneous. Experimental results show that the model is robust to initialization. As can be seen from the segmentation results of noise images, our model can resist the influence of noise compared with CV model, LBF model, LIC model, ALFB model and fractional differential with fixed order 1.5 and 0.5. At the same time, by comparing the segmentation results of actual images, it can be clearly seen that our model can obtain finer edge contour.

Author Contributions: Conceptualization, Y.Z.; Data curation, Y.T.; Methodology, Y.Z.; Validation, Y.T.; Writing—original draft, Y.T. All authors have read and agreed to the published version of the manuscript.

Funding: This study was funded by the Key Research Project of the Henan Provincial Higher Education under Grants No.20A510011 and the Key R&D and promotion projects in Henan Province under Grants No.192102210093.

Informed Consent Statement: Informed consent was obtained from all subjects involved in the study. Written informed consent has been obtained from the patient(s) to publish this paper.

Conflicts of Interest: The authors declare no conflict of interest.

References

1. Li, M.M.; Li, B.Z. A Novel Active Contour Model for Noisy Image Segmentation Based on Adaptive Fractional Order Differentiation. *IEEE Trans. Image Process.* **2020**, *29*, 9520–9531. [CrossRef]
2. Ren, Z.M. Adaptive active contour model driven by fractional order fitting energy. *Signal Process.* **2015**, *117*, 138–150. [CrossRef]
3. Chen, B.; Huang, S.A.; Liang, Z.C.; Chen, W.; Pan, B.B. A fractional order derivative based active contour model for inhomogeneous image segmentation. *Appl. Math. Model.* **2019**, *65*, 120–136. [CrossRef]
4. Mathieu, B.; Melchior, P.; Oustaloup, A. Fractional differentiation for edge detection. *Signal Process.* **2003**, *83*, 2421–2432. [CrossRef]
5. Zhang, Y.S.; Zhang, F.; Li, B.Z. Image restoration method based on fractional domain variable order differential. *Multidimens. Syst. Signal Process.* **2018**, *29*, 999–1024. [CrossRef]
6. Zhang, Y.S.; Zhang, F.; Li, B.Z.; Tao, R. Fractional domain varying-order differential denoising method. *Opt. Eng.* **2014**, *53*, 102102. [CrossRef]
7. Zhang, Y.S.; Zhang, F.; Lu, M. Relationship between fractional calculus and fractional Fourier transform, SPIE Optical Engineering + Applications. In *Signal and Data Processing of Small Targets*; International Society for Optics and Photonics: Bellingham, WA, USA, 2015.
8. Caselles, V.; Kimmel, R.; Sapiro, G. Geodesic active contours. *Int. J. Comput. Vis.* **1997**, *62*, 61–79. [CrossRef]
9. Kass, M.; Witkin, A.; Terzopoulos, D. Snakes: Active contour models. *Int. J. Comput. Vis.* **1988**, *1*, 321–331. [CrossRef]
10. Feng, R.J.; Hui, Y.J. Edge based level set with gaussian filtering regularized and its application in liver segmentation. *Adv. Mater. Res.* **2010**, *121*, 222–227. [CrossRef]
11. Khadidos, A.; Sanchez, V.; Li, C.T. Weighted Level Set Evolution Based on Local Edge Features for Medical Image Segmentation. *IEEE Trans. Image Process.* **2017**, *26*, 99. [CrossRef]
12. Liu, C.; Liu, W.; Xing, W. A weighted edge-based level set method based on multi-local statistical information for noisy image segmentation. *J. Vis. Commun. Image Represent.* **2019**, *59*, 89–107. [CrossRef]
13. Chan, T.F.; Vese, L.A. Active Contours without Edges. *IEEE Trans. Image Process.* **2001**, *10*, 266–277. [CrossRef]
14. Vese, L.A.; Chan, T.F. A Multiphase Level Set Framework for Image Segmentation Using the Mumford and Shah Model. *Int. J. Comput. Vis.* **2002**, *50*, 271–293. [CrossRef]
15. Tsai, A.; Yezzi, A.; Willsky, A.S. Curve evolution implementation of the Mumford-Shah functional for image segmentation, denoising, interpolation, and magnification. *IEEE Trans. Image Process.* **2001**, *10*, 1169–1186. [CrossRef] [PubMed]
16. Mumford, D.; Shah, J. Optimal approximations by piecewise smooth functions and associated variational problems. *Commun. Pure Appl. Math.* **1989**, *42*, 577–685. [CrossRef]
17. Li, C.M.; Kao, C.Y.; Gore, J.C.; Ding, Z. Implicit Active Contours Driven by Local Binary Fitting Energy. In Proceedings of the 2007 IEEE Conference on Computer Vision and Pattern Recognition, Minneapolis, MN, USA, 17–22 June 2007; pp. 1–7.
18. Zhang, K.; Zhang, L.; Lam, K.M.; Zhang, D.A. Level Set Approach to Image Segmentation with Intensity Inhomogeneity. *IEEE Trans. Cybern.* **2017**, *46*, 546–557. [CrossRef] [PubMed]

19. Liu, S.; Peng, Y. A local region-based Chan-Vese model for image segmentation. *Pattern Recognit.* **2010**, *43*, 603–618. [CrossRef]
20. Wang, X.F.; Huang, D.S.; Xu, H. An efficient local Chan-Vese model for image segmentation. *Pattern Recognit.* **1997**, *62*, 61–79. [CrossRef]
21. Ma, D.; Liao, Q.; Chen, Z.; Ran, L.; Ma, H. Adaptive local-fitting-based active contour model for medical image segmentation. *Signal Process. Image Commun.* **2019**, *76*, 201–213. [CrossRef]
22. Peng, Y.; Liu, S.; Qiang, Y.; Wu, X.J.; Hong, L. A local mean and variance active contour model for biomedical image segmentation. *J. Comput. Sci.* **2019**, *33*, 11–19. [CrossRef]
23. Li, C.M.; Xu, C.; Gui, C.; Martin, D. Fox. Distance Regularized Level Set Evolution and Its Application to Image Segmentation. *IEEE Trans. Image Process.* **2010**, *19*, 3243–3254.
24. Li, C.M.; Huang, R.; Ding, Z.H.; Gatenby, J.C.; Metaxas, D.N.; Gore, J.C. A Level Set Method for Image Segmentation in the Presence of Intensity Inhomogeneities with Application to MRI. *IEEE Trans. Image Process.* **2010**, *19*, 3243–3254.
25. Gilles, A.; Pierre, K. *Mathematical Problems in Image Processing: Partial Differential Equations and the Calculus of Variations*; Springer: New York, NY, USA, 2002.